Inviscid Flowfield Calculations for Re-entry Vehicles with Control Surfaces

J. M. Solomon,* M. Ciment,† R. E. Ferguson,† and J. B. Bell†
Naval Surface Weapons Center/White Oak Laboratory, Silver Spring, Md.

This paper discusses various methods that were developed for use in a computer code which predicts the aerodynamic characteristics of inviscid supersonic flow on realistic re-entry vehicle shapes, including cuts and flaps. Numerical techniques are developed for the treatment of: 1) boundary conditions on the body surface and at the bow shock wave, 2) flow nonuniformities which appear at sharp corners in the body geometry, and 3) large entropy variations that develop downstream near the surface on a blunted configuration. Example computations are presented to illustrate the utility of these techniques.

I. Introduction

THE numerical calculation of the inviscid flowfield over re-entry vehicles is conveniently divided into two parts (see Fig. 1): 1) the *blunt body region* where the axial component of the flow is subsonic/transonic and 2) the *supersonic region* where the axial component of the flow is supersonic (see Refs. 1-6). This latter portion represents the majority of the total flowfield on maneuverable and high-performance ballistic re-entry vehicles.

This paper is devoted to the consideration of the supersonic region calculation. In this region, the governing equations are hyperbolic with the body axis as the time-like direction. This implies, among other things, that the numerical solution can be obtained by marching stepwise in the z direction. Computational codes which are currently in practicable use for this problem employ finite-difference techniques based on MacCormack's scheme[7,8] and treat the bow shock wave as an unknown (free) boundary (e.g., Refs. 1-6). The existing codes were developed for smooth body geometries. Several[2,4,5] have the capability of treating embedded shock waves which may develop in the interior of the shock layer.

In these existing codes a variety of procedures have been used for the numerical treatment of the boundary conditions at the body wall and the bow shock (see Ref. 9 for a survey). In applications involving advanced re-entry vehicle shapes, the treatment of the body wall conditions is complicated by the large entropy gradient (entropy layer) which generally appears at the body surface. In this paper, a form of the wall boundary conditions is presented which enables accurate computations in the presence of a wall entropy layer without the use of special logic or heuristic computational devices. These boundary conditions and those for use at the bow shock boundary are derived (see Sec. IV) using characteristic theory in the spirit of Kentzer.[10]

Most re-entry configurations of practical interest have sharp corners or edges such as found on segmented bodies (e.g., biconics) and bodies with aerodynamic control surfaces formed by cuts and flaps. Sharp corners can produce nonuniformities such as shock waves or expansion fans which are attached directly to the body surface. This is in contrast to the situation treated by existing methods where the body is smooth and such nonuniformities form away from the body surface (generally, several mesh points). To treat *attached* discontinuous flows it is necessary to develop localized procedures which allow the nonuniformity to develop properly at the wall, and propagate into the interior. In this paper, local procedures are developed for certain corner problems (see Sec. V). For our purposes these procedures have been incorporated into a shock capturing technique similar to that of Kutler et al.[5] These procedures however can be readily adapted for use in a shock tracking approach.

The numerical methods discussed in this paper have been implemented into a computer code for predicting supersonic flowfields and inviscid aerodynamic coefficients on arbitrary shaped re-entry bodies in pitch and yaw with either perfect gas or equilibrium air thermodynamics. A complete description of this code with details of the analytical background is given in Ref. 11.

II. Governing Equations and Boundary Conditions

With respect to the cylindrical coordinate system r,ϕ,z illustrated in Fig. 1, the conservation of mass and momentum equations for a steady, inviscid flow can be written as a system of (weak) conservation laws; i.e.,

$$\frac{\partial U}{\partial z}+\frac{\partial \mathcal{F}}{\partial r}+\frac{\partial \mathcal{G}}{\partial \phi}+\mathcal{E}=0 \tag{1}$$

where the vectors U, $\mathcal{F}$,$\mathcal{G}$, and $\mathcal{E}$ are given by

$$U=(\rho w,\ p+\rho w^2,\ \rho wu,\ \rho wv)^t$$

$$\mathcal{F}=(\rho u,\ \rho wu,\ p+\rho u^2,\ \rho wv)^t$$

$$\mathcal{G}=1/r(\rho v,\ \rho vw,\ \rho vu,\ p+\rho v^2)^t$$

$$\mathcal{E}=1/r(\rho u,\ \rho uw,\ \rho(u^2-v^2),\ 2\rho uv)^t$$

where t denotes transpose, p is the pressure, ρ is the density, and u,v,w are the velocity components in the r,ϕ,z directions, respectively. The energy equation for a steady inviscid flow with an isoenergetic freestream can be reduced to an algebraic equation

$$h+\tfrac{1}{2}(u^2+v^2+w^2)=H_\infty\equiv h_\infty+\tfrac{1}{2}(u_\infty^2+v_\infty^2+w_\infty^2) \tag{2}$$

Here h is the enthalpy, and H_∞ is the total energy in the freestream (which is constant). The gas is assumed to be in local thermodynamic equilibrium so that known relationships exist between the thermodynamic variables p,ρ,h,a (the sound speed), and s (the entropy). The latter two variables will be needed later.

Presented as Paper 77-84 at the AIAA 15th Aerospace Sciences Meeting, Los Angeles, Calif., Jan. 24-26, 1977; submitted Feb. 7, 1977; revision received July 21, 1977.

Index categories: Computational Methods; Supersonic and Hypersonic Flow; Entry Vehicle Dynamics and Control.

*Research Mathematician, Mathematics and Engineering Analysis Branch. Member AIAA.

†Mathematician, Mathematics and Engineering Analysis Branch.

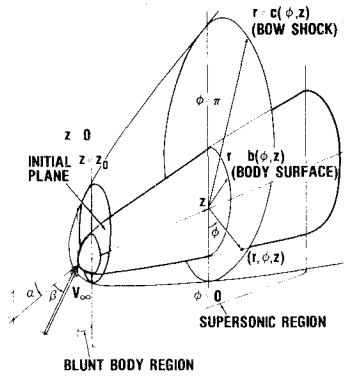

Fig. 1 Computational regions and cylindrical coordinate system for inviscid flow calculations.

The shock layer is bounded by the given body surface, prescribed as $r=b(\phi,z)$, and the bow shock wave, $r=c(\phi,z)$, which is an unknown to be determined. On the body surface, the boundary condition for inviscid flow requires that the normal component of velocity must vanish, i.e.,

$$u-b_z w-(b_\phi/b)v=0 \tag{3}$$

On the bow shock surface the Rankine-Hugoniot relations must hold. These relations are

$$\rho V_n=\rho_\infty V_{n_\infty},\quad p+\rho V_n^2=\rho_\infty+\rho_\infty V_{n_\infty}^2 \tag{4a}$$

$$h+\tfrac{1}{2}V_n^2=h_\infty+\tfrac{1}{2}V_{n_\infty}^2,\quad \boldsymbol{V}-\boldsymbol{n}V_n=\boldsymbol{V}_\infty-\boldsymbol{n}V_{n_\infty} \tag{4b}$$

$\boldsymbol{V}$ is the velocity vector, $V_n=\boldsymbol{n}\cdot\boldsymbol{V}$ is the component of velocity normal to the shock surface, and $\boldsymbol{n}$ is the unit vector normal to the shock surface; i.e., in the direction of grad$[c(\phi,z)-r]$. The subscript ∞ refers to the freestream quantities (upstream of the shock); all other quantities are values immediately behind (downstream of) the shock.

III. Review of Computational Procedure

The region to be considered is $z\geq z_0$ where $z=z_0$ is some plane in the supersonic region where all flow quantities and shock geometry are known. Two different problems will be considered; the symmetric and the nonsymmetric problems. In the symmetric problem, the body is assumed to be symmetric about the pitch plane and $\beta=0$ (see Fig. 1). The calculation for this problem is performed for $0\leq\phi\leq\pi$ since the flowfield is symmetric about $\phi=0$ and $\phi=\pi$ (wind and lee sides, respectively). In the nonsymmetric problem, the body need not be symmetric and/or $\beta\neq0$. In this problem, the calculation must be performed for $0\leq\phi\leq2\pi$.

For both problems, the shock layer for $z\geq z_0$ is transformed into the computational region $Z\geq z_0$, $0\leq X\leq1$, $0\leq Y\leq1$. The transformation is conveniently expressed as a composite of two mappings. The first is the usual normalizing transformation

$$\bar{x}=[r-b(z,\phi)]/[c(z,\phi)-b(z,\phi)] \tag{5a}$$

$$\bar{y}=\phi/\phi_0,\quad \bar{z}=z \tag{5b}$$

where ϕ_0 is π for the symmetric problem and 2π for the nonsymmetric problem. The primary purpose of the second mapping is to cluster computational points in the shock layer while retaining a uniform grid in the computational space. It is convenient to express this mapping in inverted form

$$\bar{x}=f(X,Y,Z),\quad \bar{y}=g(Y,Z),\quad \bar{z}=Z \tag{6}$$

where $f(0,Y,Z)=0$, $f(1,Y,Z)=1$; $g(0,Z)=0$, $g(1,Z)=1$. Apart from these boundary conditions (and certain restrictions mentioned later in this section), the mapping functions f and g can be arbitrary, provided that the functions and their derivatives up to an including the second order are smoothly defined. Clustering functions of this type with f and g defined analytically using transcendental functions have been used previously.[1,5,12] Another approach, which we have found to be convenient in a variety of applications, is to allow the user to input as data the values of $\bar{x}$ and $\bar{y}$ which are to correspond to the computational mesh. Although the functions f and g are implicitly defined, the required derivatives can be obtained directly by second-order accurate finite-difference formulas (see Ref. 11 for details).

The governing equations Eq. (1), when transformed to the computational space (X,Y,Z) by Eqs. (5) and (6) become

$$\frac{\partial U}{\partial Z}+\frac{\partial F}{\partial X}+\frac{\partial G}{\partial Y}+E=0 \tag{7}$$

where the vectors F, G, and E are given by

$$F=X_z U+X_r\mathcal{F}+X_\phi\mathcal{G},\quad G=Y_z U+Y_\phi\mathcal{G} \tag{8}$$

$$E=\mathcal{E}-[(\frac{\partial X_z}{\partial X}+\frac{\partial Y_z}{\partial Y})U+\frac{\partial X_r}{\partial X}\mathcal{F}+(\frac{\partial X_\phi}{\partial X}+\frac{\partial Y_\phi}{\partial Y})\mathcal{G}] \tag{9}$$

The quantities Y_z, X_z, X_r, X_ϕ, and Y_ϕ and their partial derivatives can be expressed in terms of b, c, g, and f and their partial derivatives using Eqs. (5) and (6) (see Ref. 11).

The system of partial differential equations, Eq. (7), is discretized and solved numerically in the computational space using a mesh defined by

$$\{(X_n,Y_m):X_n=(n-1)\Delta X(n=1,2,\ldots,N),$$

$$Y_m=(m-1)\Delta Y(m=1,2,\ldots M)\}$$

where $\Delta X=1/(N-1)$, and $\Delta Y=1/(M-1)$. We assume that the quantities ρ,u,v,w,p,c_ϕ,c_z are known for $Z=Z^k$ on the mesh defined above. The objective is to determine these quantities on this mesh for $Z=Z^{k+1}=Z^k+\Delta Z$. There are four types of points, each requiring differing numerical procedures; interior points corresponding to $n=2,\ldots,N-1$; $m=2,\ldots,M-1$; points on the symmetry or periodic boundary planes $Y=0$ and $Y=1$ ($m=1$ and $m=M$, respectively); boundary points at the bow shock, $X=1$ $(n=N)$; boundary points at the body surface, $X=0$ $(n=1)$. For all points, the solution is advanced using predictor-corrector finite-difference methods. The boundary points on $X=0$ are discussed in Sec. IV.

The numerical solution for interior points is similar to that of Kutler et al.[5] Standard forms of the MacCormack scheme applied to Eq. (7) are used to advance the conservation vector, U (for details see Ref. 5 or 11). The flow variables p,ρ,u, etc. are determined from the equation defining U using Eq. (2) and the equation of state $h=h(p,\rho)$ (see Ref. 5 or 11).

The interior and boundary schemes (see Sec. IV) are implemented at the symmetry (or periodic) boundaries $Y=0$ and $Y=1$ in the standard manner. That is, "fringe" planes $Y=-\Delta Y$ and $Y=1+\Delta Y$ (or $Y=1$) are introduced on which quantities needed in the Y differences are defined using symmetry (or periodic) conditions. Additional considerations come into play when clustering transformations are used. To maintain second-order accuracy with convenient representation of variables, special restrictions must be placed on the f and g as a function of Y (see Ref. 11).

The step size ΔZ must be restricted in order to insure numerical stability of the MacCormack scheme. We derived a stability condition based on a comparison of the domain of dependence of the "linearized" partial differential equations with that of the finite-difference equations.[11] We used this condition with a multiplicative safety factor of 0.9. This type of stability condition has been found to be adequate for the

present problem[13]; however, it should be pointed out that geometric conditions of this type, although necessary for stability, are not sufficient to guarantee stability of the MacCormack scheme in general (see Ref. 14).

IV. Boundary Conditions

In general, the numerical solution of mixed initial-boundary value problems of the present type are complicated by the necessity of providing proper numerical approximations at the boundaries. Clearly, the given flow boundary conditions Eqs. (3) and (4) on $X=0$ and $X=1$, respectively, must be satisfied. However it is necessary to supplement these boundary conditions with appropriate numerical approximations at the boundaries obtained from the governing partial differential equations. It has long been recognized that for hyperbolic systems, numerical approximations at the boundaries can be derived by appealing to certain compatibility relations from the theory of characteristics. Clearly, one starts with *admissible* characteristic relations; i.e., compatibility relations associated with bicharacteristic directions pointing from the boundary into the solution domain in the backward time-like direction (negative Z for the present problem). Kentzer,[10] in the context of unsteady flows, suggested how the characteristic relations can be conveniently utilized in a finite-difference solution. Observing that attempts to utilize characteristic directions inevitably requires interpolation from the underlying finite-difference mesh, Kentzer suggests using the admissible characteristic relations together with the given boundary conditions to form a system of partial differential equations on the boundary. This system is solved using a finite-difference method.

Several papers have reported using this type of approach for the steady equations. Our characteristic analysis is detailed in Ref. 11. However, some remarks on the derivation are in order here. To obtain a characteristic compatibility condition of the full system it is essential to use all three momentum equations plus the continuity equation. For example, the characteristic compatibility conditions developed for a reduced system (e.g., as in Ref. 15) do not result in a characteristic compatibility relationship for the complete system. In the following we limit our discussion to several salient features of the resulting numerical boundary conditions at the wall and shock.

Wall Boundary Points $X=0$

On the boundary $X=0$, the boundary condition in Eq. (3) must be satisfied. The characteristic analysis for this boundary indicates there are three independent *admissible* characteristic relations. Two relations correspond to the streamline and one corresponds to the Mach conoid. These relations can be written on $X=0$ using Eq. (3) in the form

$$w\frac{\partial s}{\partial Z} = -\left(Y_z w + Y_\phi \frac{v}{r}\right)\frac{\partial s}{\partial Y} \tag{10}$$

$$\frac{\partial V_2}{\partial Z} = R_1,\quad V_2 = v + b_\phi \frac{u}{b} \tag{11}$$

$$\beta_1 \frac{\partial p}{\partial Z} = -\lambda_+\left(\beta_1 \frac{\partial p}{\partial X} - \rho w \frac{\partial A}{\partial X}\right) + R_2 \tag{12}$$

where

$$A = X_z w + X_r u + X_\phi v/r \tag{13}$$

and $\beta_1 > 0$, $\lambda_+ < 0$ contain undifferentiated quantities, and R_1 and R_2 contain Y partial derivatives and undifferentiated quantities.

Since w and β_1 are positive, Eqs. (10-12) can be used to advance s, V_2, and p along $X=0$ in a MacCormack type predictor-corrector method. In this scheme, the Z derivatives are determined using Eqs. (10-12) with the Y derivatives approximated by the usual alternating first-order forward-backward differences and the X derivatives approximated by one-sided differences. When the X differences are first order in both the predictor and corrector, the method is formally first-order accurate. To obtain second-order accuracy, an additional term is added in the corrector (see e.g., Ref. 16). For smooth body geometries, the second-order formulation is desirable. However, when the body has discontinuous slopes and/or curvatures, the first-order formulation is superior in the downstream vicinity of the dicontinuity due to the lack of smoothness in the flowfield near the body. For this reason, both formulations are available in the present code. After the predicted (or corrected) values of s, V_2, and p are determined, the predicted (or corrected) values of all remaining flow variables are obtained using Eqs. (2, 3, and 11) and the equations of state $\rho=\rho(p,s)$ and $h=h(p,\rho)$. Note that the boundary condition in Eq. (3) is satisfied in both the predictor and corrector steps.

The form of the pressure equation given by Eq. (12) has an advantage over previous forms of this equation in that it allows one to maintain an accurate approximation even when a flow nonuniformity develops and remains along the body surface (e.g., entropy layers on blunted slender bodies). Other formulations which utilize finite differencing in the vicinity of such nonuniformities, generally, difference flow quantities which are not smooth in the X direction and hence require some local modifications to maintain the calculation. In our formulation, *only smooth quantities are differenced in the X direction*. To see this, first observe that, since such nonuniformities lie along the body surface which is a stream surface, they have the character of a contact discontinuity. It is known (Ref. 17, pp. 317-18) that across such a discontinuity only the pressure and the normal component of velocity can never experience jumps. Now consider the present wall point computation. The only X differences required are in Eq. (12), the equation for pressure. The quantities V_2 and s are advanced using only quantities defined on the wall. Further, the only quantities differenced in the X direction are p and A. But, p is smooth across the nonuniformity, and A at the wall is, except for a factor involving geometry, the normal component of velocity [see Eq. (13)] which is also smooth across the nonuniformity. Hence, the wall point calculation remains well behaved, in fact, second-order differencing in the X direction is still meaningful across a nonuniformity of this type. In this regard it is interesting to consider the influence of the wall calculation on the interior point calculation. Since $A=0$ on $X=0$ in both the predictor and corrector steps, it can be shown[8] that for any MacCormack scheme the pressure is the only surface flow variable that affects the interior point calculation. Thus, the interior points are unaffected by the nonuniformity if the surface pressure is computed correctly.

In the calculation of blunted smooth body shapes, the present scheme maintains the wall entropy at the stagnation point value (i.e., the correct inviscid value); see Eq. (10). The scheme is inherently capable, without the use of special numerical adjustment, of accurate calculations while maintaining the correct inviscid value of wall entropy even when a strong entropy layer develops. In practical calculations, the entropy layers cannot be fully resolved numerically because ultimately the layer's thickness will become smaller than the radial mesh spacing that one can afford to employ on any computer. When this happens, the present scheme produces a contact discontinuity at the body surface which corresponds to the variation of the flow variables across the entropy layer.

The development of the entropy layer and the corresponding numerical discontinuity produce at the body surface a flow with higher entropy and lower Mach number than the adjacent interior flow. This has at least two im-

portant effects on the calculation. First, the low axial Mach number at the surface causes the stability condition to select a step size ΔZ which is smaller than if the wall entropy were at a level corresponding to the adjacent interior flow. Second, the lower-speed flow on the wall can, in the presence of local compressions near the wall, become locally subsonic in the axial direction even though the adjacent interior flow remains supersonic. The former effect increases computer time; the latter causes premature termination of the calculation.

It is therefore expedient in some cases to reduce the wall entropy and thereby reduce or eliminate the entropy layer. The procedure for performing this given by Kyriss and Harris[6] is incorporated as an option in the present code. The method is basically to define the wall entropy by linear extrapolation from the interior points rather than by numerically integrating Eq. (10). This procedure gradually reduces the wall entropy and ultimately eliminates the numerical entropy discontinuity at the wall. Because of the heuristic nature of this procedure, general conclusions concerning its use cannot be made at this time. Calculations for sphere-cones with and without the wall entropy reduction option indicate that only the surface flow variables (except pressure) are changed; see Sec. VI for an example comparison. The procedure has more effect near discontinuities of body slope (this will be discussed in Sec. V).

Shock Boundary Points ($X=1$)

On the boundary $X=1$, the Rankine-Hugoniot conditions in Eq. (4) must be satisfied. The characteristic analysis of this boundary indicates that there is only one admissible characteristic relation (corresponding to the Mach conoid). On $X=1$ this relation takes the form

$$\beta_1 \frac{\partial p}{\partial Z} + \rho X_r [w \frac{\partial u}{\partial Z} - u \frac{\partial w}{\partial Z} - \frac{c_\phi}{c} (w \frac{\partial v}{\partial Z} - v \frac{\partial w}{\partial Z})] = R_3 \quad (14)$$

where $\beta_1 > 0$ contains undifferentiated quantities, and R_3 contains both X and Y partial derivatives and undifferentiated quantities. The direct use of Eq. (14) simultaneously with the shock relations of Eq. (4) requires an iterative procedure even for a perfect gas. A more direct numerical method is obtained when Eq. (14) is rewritten using the shock relations and the equation of state to evaluate the Z derivatives appearing in Eq. (14) in terms of the shock shape function, c and its derivatives. After these manipulations, Eq. (14) can be expressed in the form

$$C_1 \frac{\partial c_z}{\partial Z} + C_2 \frac{\partial (c_\phi / c)}{\partial Z} = R_4 \quad (15)$$

where R_4 has the same general form as R_3, and the coefficients C_1 and C_2 involve undifferentiated flow quantities and the shock geometry c, c_ϕ, c_z. In addition to Eq. (14), we also have

$$\frac{\partial c}{\partial Z} = c_z - (\frac{Y_z}{Y_\phi}) c_\phi \quad (16)$$

and

$$\frac{\partial c_\phi}{\partial Z} = Y_\phi \frac{\partial c_z}{\partial Y} - Y_z \frac{\partial c_\phi}{\partial Y} \quad (17)$$

The former is the chain rule for the Z derivative of the shock shape function $c(\phi, z)$; the latter relation expresses, through the chain rule, that $c_{z\phi} = c_{\phi z}$.

When the coefficient C_1 is nonzero, Eqs. (15-17) determine the Z derivatives of the shock geometry functions c, c_ϕ, and c_z in terms of X and Y derivatives and inhomogeneous terms. Thus, c, c_ϕ, and c_z can be advanced using a predictor-corrector method of the MacCormack form where the Z derivatives are obtained using Eqs. (15-17) with the Y derivatives approximated by alternating first-order forward-backward differences and the X derivatives approximated by a one-sided second-order scheme of the form given in Ref. 16. After the predicted (or corrected) values of c, c_ϕ, and c_z are determined, the corresponding flow quantities on $X=1$ are obtained from the shock relations in Eq. (4) in the well-known manner. Note that in this scheme the shock relations are satisfied in both the predictor and corrector steps. As previously mentioned, to use this scheme it is required that the coefficient C_1 does not vanish anywhere on the bow shock. It can be proved[11] that this is indeed the case for a perfect gas when $w > a$. Our computational experience indicates that this is also true for air in thermodynamic equilibrium.

The present scheme for the shock points has been compared with the scheme originally proposed by Thomas et al.[1] and modified for use in a conservation method by Kutler et al.[5] The principal differences between the schemes is that the Thomas-Kutler method is not based on (or consistent with) the theory of characteristics. In general, both methods appear to have the same truncation error, that is, they provide similar results within an expected error range. However, in certain cases of high angle of attack, the Thomas-Kutler scheme is poorly behaved and exhibits what looks like a mild instability. The present scheme shows no such difficulties. An example calculation showing this phenomenon is given in Sec. VI

V. Bodies with Discontinuous Slopes

Re-entry vehicle shapes such as biconics, flared bodies, and bodies with control surface cuts and flaps are most accurately described, for the purposes of our code, by *piecewise* analytical functions. Thus, the body shape function, $b(z, \phi)$, may contain discontinuities in b_z and b_ϕ. These discontinuities exist along certain surface curves which we will refer to as *edges*. Generally, along such an edge there will be discontinuities in the surface flow variables appearing as either shock waves or expansion fans attached to the body surface along the edge. The basic marching procedure described in Secs. III and IV and those of existing codes, being developed for smooth bodies, do not account for the appearance of flow discontinuities at the body surface. These methods, when marched across edges without special provisions, at best spread the discontinuities over several marching steps. When the discontinuities are not small, numerical oscillations occur which can result in a program halt or, at the very least, a substantial region of unrealistic results. A procedure has been developed and incorporated in the present code which, in most instances, numerically models the appearance of surface flow discontinuities at edges. The basic idea is to locate an edge as it is encountered in the marching process and insert in the calculation the associated jumps in the surface flow variables based on a local analysis of the inviscid supersonic flow across the edge. For inclusion in our code, this idea is implemented in an approximate manner with the objective of keeping the computer time to a minimum. We have found that in most cases the present procedure yields, without noticeable increase in computer time, far better results than would be obtained by simply marching across the edge. After our paper was presented, we were made aware of the recent work of Colasurdo and Pandolfi[18] which independently suggests a basically similar approach for three-dimensional expansion corners.

For complicated geometries (e.g., bodies with slices), the precise location of edges would require a considerable amount of additional logic and computations. To avoid this, we only locate edges approximately; i.e., within at most ΔZ. The procedure is as follows. At every step, $Z^{k+1} = Z^k + \Delta Z$, the values of b_z and b_ϕ are compared to their previous values (at Z^k) using

$$|(b_z)_m^k - (b_z)_m^{k+1}| - \Delta Z \max\{|(b_{zz})_m^k|, |(b_{zz})_m^{k+1}|\} > \epsilon$$

$$|(b_\phi)_m^k - (b_\phi)_m^{k+1}| - \Delta Z \max\{|(b_{\phi z})_m^k|, |(b_{\phi z})_m^{k+1}|\} > \epsilon$$

where ϵ is a small positive number (we use $\epsilon = 10^{-6}$). When *either* of these inequalities is satisfied, a discontinuity in b_z and/or b_ϕ is assumed to exist between Z^k and Z^{k+1} at $Y = Y_m$ (i.e., an edge is assumed to be crossed by the mesh line $Y = Y_m$ between Z and Z^{k+1}). At each such value of Y, the body geometry is temporarily modified‡ at Z^{k+1} by putting the body shape derivatives $b_z, b_\phi, b_{zz}, b_{z\phi}$, and $b_{\phi\phi}$ equal to their values at Z^k. This temporarily removes the discontinuities in the body slopes and the predictor-corrector sequence for the "modified body" is performed for the step Z^{k+1}. After the corrector step, the body derivatives which were modified are put equal to their true values at Z^{k+1}. The edge is thereby relocated at Z^{k+1}. Note that, in the present procedure, edges are given special consideration *only* when a Y mesh line crosses the edge in the marching direction.

Let us now turn to the procedure for determing the appropriate flow discontinuities at the points $(0, Y_m, Z^{k+1})$ where the edge has been placed. Let (r_0, ϕ_0, z_0) where $r_0 = b(\phi_0, z_0)$ be the body surface point corresponding to $(0, Y_m, Z^{k+1})$. We first discuss our treatment of the case where the flow on the surface of the "modified body" crosses the edge in the marching direction. Here, the "modified body" geometry will be referred to as the *upstream* side of (r_0, ϕ_0, z_0) and the true body geometry as the *downstream* side of (r_0, ϕ_0, z_0). All flow quantities on the upstream side of $(r_0 n \phi_0, z_0)$ are the computed values at this point using the modified geometry and thus are known. The resulting problem is to determine the surface flow quantities on the downstream side of (r_0, ϕ_0, z_0) given the upstream flow and the body slopes on both sides. At (r_0, ϕ_0, z_0), there are two distinct body normal vectors, denoted by n_+ and n_-. Here and throughout this section the subscripts $-$ and $+$ denote quantities associated with the upstream and downstream sides of (r_0, ϕ_0, z_0), respectively. We introduce two sets of mutually orthogonal unit vectors, one for each side of (r_0, ϕ_0, z_0), given by (see Fig. 2)

$$\eta_\pm = n_\pm / |n_\pm|, \quad \tau = \eta_+ \times \eta_-, \quad \sigma_\pm = \eta_\pm \times \tau \tag{18}$$

The vector τ is tangent to the edge at (r_0, ϕ_0, z_0). The edge flow problem is characterized by the value of $q_- = V_- \cdot \sigma_-$, the known upstream component of the surface velocity normal to the edge. Since by computation the upstream flow satisfies the boundary condition $V_- \cdot \eta_- = 0$, it follows from Eq. (18) that

$$q_- = (V_- \cdot \eta_+) / \sqrt{1 - (\eta_- \cdot \eta_+)^2} \tag{19}$$

When the upstream flow normal to the edge is supersonic or sonic (i.e., $|q_-| \geq a_-$), the flow in a small neighborhood of (r_0, ϕ_0, z_0) has been analyzed by Prandtl and Meyer (see, e.g., Ref. 17, Chap. XI). This analysis indicates that near (r_0, ϕ_0, z_0) there is no change in the velocity component tangent to the edge; i.e.,

$$V_- \cdot \tau = V_+ \cdot \tau \tag{20}$$

Further, the quantities $p_+, \rho_+, q_+ = V_+ \cdot \eta_+$ are given by the classical two-dimensional supersonic turning relations in the plane determined by η_+ and η_-. The angle through which the flow is turned is given by

$$\theta = \cos^{-1}(\eta_+ \cdot \eta_-) \tag{21}$$

There are two possible cases, $q_- > 0$ and $q_- < 0$. When $q_- > 0$, it follows from Eq. (19) that $(V_- \cdot \eta_+) > 0$; and, thus, the flow is turned by a centered expansion fan attached to the edge. When $q_- < 0$, it follows that $(V_- \cdot \eta_+) < 0$, and the flow is turned by an oblique shock wave attached to the edge. In both cases, the relations which express $p_+ \rho_+$, and $|q_+|$ in terms of $\theta, p_-, \rho_-, |q_-|$ are well known. The downstream velocity is obtained, using Eq. (21) and the fact that $V_+ \cdot \eta_+ = 0$, as

$$V_+ = (V_- \cdot \tau)\tau + q_+ \sigma_+ \tag{22}$$

In the case when $V_- \cdot \eta_+ < 0$, it can happen that conditions are such that no oblique shock wave exists; this can occur, for example, when θ is large and/or $(q_-/a_-)^2$ is near one. In this situation, the Prandtl-Meyer analysis breaks down and a semiempirical procedure is used; namely, a normal shock wave (i.e., normal to σ_-) is assumed to exist on the upstream side in front of (r_0, ϕ_0, z_0). The flow quantities behind this normal shock are obtained in terms of $|q_-|, p_-, \rho_-$ (the flow variables in front of the shock) in the standard manner. The final results for p_+, ρ_+, and $|q_+|$ are obtained by performing an isentropic expansion from the normal shock values through the turning angle, θ, using the modified Newtonian pressure law (i.e., the sine-squared rule).

On complicated body shapes, there can arise edge problems for which the foregoing analysis does not apply. Such cases occur when the upstream flow normal to the edge is subsonic (i.e., when $|q_-| < a_-$) or when the upstream flow does not cross the edge in the marching direction. In the absence of a rational approach for these cases, we use the following heuristic procedure. We assume that there is no change in the velocity component tangent to the edge, and further, that the velocity vector is rotated to satisfy $V_+ \cdot \eta_+ = 0$ with no jumps in pressure, density, and magnitude of velocity across the edge (i.e., $p_+ = p_-, \rho_+ = \rho_-, |q_-| = |q_+|$). The downstream velocity components are determined using Eq. (22). This procedure is essentially equivalent to marching directly across the edge with no special provisions.

When an edge is encountered in the marching procedure, the computed surface flow variables for the modified geometry are replaced by the downstream flow variables determined from the foregoing procedure. This is done when the modified geometry is replaced by the true geometry and before the next marching step (i.e., $Z = Z^{k+2}$). This procedure establishes discontinuities in the flow variables at the approximated edge locations. Since the basic scheme for interior points is of the dissipative conservation type, one might expect that it will, without modification, properly approximate the propagation of these flow discontinuities into the interior of the shock layer. Modifications, however, must be made in the scheme for body surface points downstream of an edge. The quantities p and A will no longer be smooth in the X direction. Under these circumstances, second-order X-differencing at the wall (see Sec. IV) is not justified, and we use the first-order scheme for the mesh lines, $Y = Y_m$, after they cross a discontinuity. Even so, the wall point calculation can be ill-behaved in a small region downstream of an expansion or compression edge when the resulting flow discontinuities are sufficiently large. The reason for this appears to be that the wall point calculation requires that X-differences be taken across a flow discontinuity. Numerical experiments reveal that until this discontinuity propagates across, at least, the first interior mesh point $(X = \Delta X)$ the numerical scheme for the wall

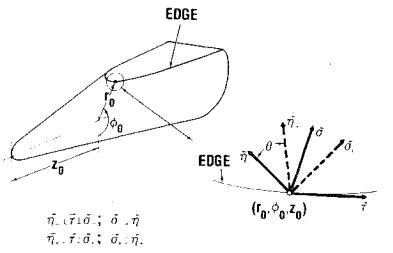

Fig. 2 Orthogonal directions used in the analysis of the flow over an edge.

‡The body that is in effect created at $Z = Z^{k+1}$ by this convention will be referred to as the "modified body."

apparently lacks sufficient dissipation to smooth out the flow. Because of this, we heuristically modify the wall point calculation in a small downstream region by multiplying the numerical X derivatives appearing in Eq. (12) by a factor which increases smoothly from zero at the edge to unity at some fixed number of marching steps downstream (we use four or less in our calculations). This heuristic procedure is used locally only for the mesh lines Y_m where an appropriate edge has been crossed. Observe that the length of the region where this procedure is employed is proportional to ΔZ; hence, it can be made as small as desired by refining the spatial mesh. At an edge which produces a compression (oblique shock), the surface value of entropy is increased across the edge. Therefore, in this case, the wall entropy reduction option (see Sec. IV) is unrealistic and should, if originally selected, be discontinued for the downstream calculation.

The preceding heuristic procedure for treating the flow downstream of an attached flow discontinuity is an expedient solution for the present body shapes of interest. The procedure is effectively $O(\Delta Z)$ in regions away from the actual discontinuity, since the modification of the Z derivatives is performed for only a fixed number of steps. Certainly, other more accurate procedures are possible but would require more computational effort. For the present procedure, the resulting comparisons with wind-tunnel and flight-test data are nonetheless quite encouraging.

VI. Numerical Results

All calculations presented here were performed for a perfect gas ($\gamma = 1.4$). The shapes considered are spherically blunted with nose radius r_n. The initial data planes were determined using an axisymmetric code[19] to compute the spherical flow in wind-oriented coordinates followed by a transformation to the body-oriented coordinates. Unless expressly stated to the contrary, all the results presented here are for zero side slip; i.e., $\beta = 0$.

To demonstrate the performance of the present code when an entropy layer develops, we have chosen as an example a 10-deg sphere-cone at a freestream Mach number, $M_\infty = 18$ and $\alpha = 1$ deg. Two calculations were performed—one using the basic wall point scheme [i.e., Eqs. (10-12)], the other using the wall entropy reduction option. Both calculations were performed using a mesh of 15 radial and 7 meridional points. The results are shown in Fig. 3 (with linear interpolation) and Fig. 4. The circles correspond to the entropy reduction option. They are shown only on $\bar{x} = 0$ since the numerical results were essentially the same for the two calculations at interior and shock points. Note that using the basic scheme, the numerical entropy discontinuity has been established at $z/r_n = 167.7$ and is maintained in the downstream calculation. Figure 4 shows that A and p are smooth across the entropy layer. The calculation using the basic scheme required 789 marching steps to reach $Z/r_n = 340$; by contrast, using wall entropy reduction, only 530 steps were required to reach this station.

As mentioned at the end of Sec. IV, the Thomas-Kutler scheme for the bow shock points is poorly behaved in certain cases. One such case is a 7-deg sphere-cone at $M_\infty = 23$, $\alpha = 25$ deg, $\beta = 1.5$ deg. Figure 5 compares the computed pressure behind the bow shock wave using the present scheme and that of Thomas-Kutler. The only difference in the computational procedures was the shock boundary scheme. The mesh used for these calculations consisted of 15 radial points and 64 unevenly distributed meridional planes (uniform $\Delta\phi = 4$ deg in the intervals 0 deg $\leq \phi \leq$ 92 deg and 262 deg $\leq \phi \leq$ 360 deg

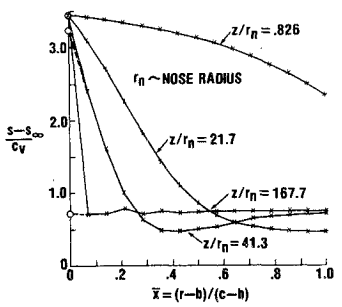

Fig. 3 Entropy distributions on $\phi = 0$ deg; 10-deg sphere-cone, $M_\infty = 18$, $\alpha = 1$ deg.

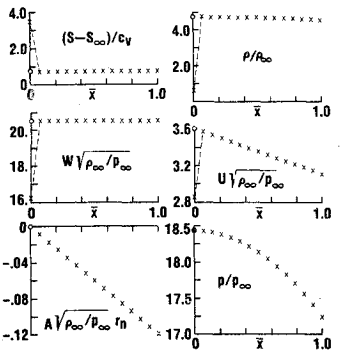

Fig. 4 Flowfield on $\phi = 0$ deg at $z/r_n = 340$; 10-deg sphere-cone, $M_\infty = 18$, $\alpha = 1$ deg.

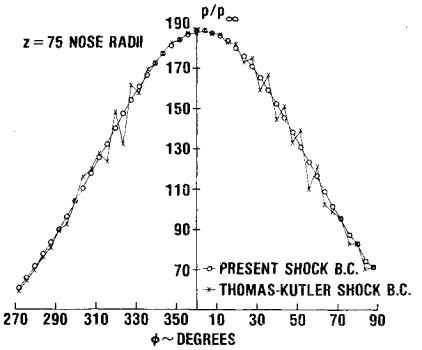

Fig. 5 Pressure at bow shock wave in the windward region; 7-deg sphere-cone, $M_\infty = 23$, $\alpha = 25$ deg, $\beta = 1.5$ deg.

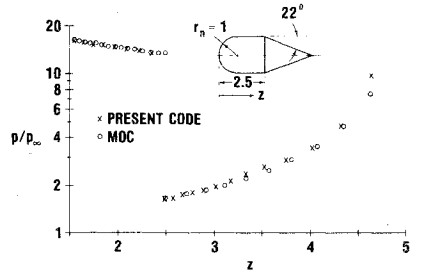

Fig. 6 Surface pressure distribution on expansion body $M_\infty = 20$, $\alpha = 0$ deg.

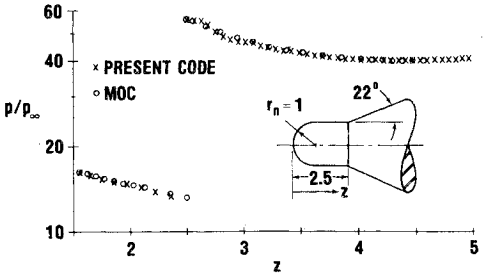

Fig. 7 Surface pressure distribution on compression body $M_\infty = 20$, $\alpha = 0$ deg.

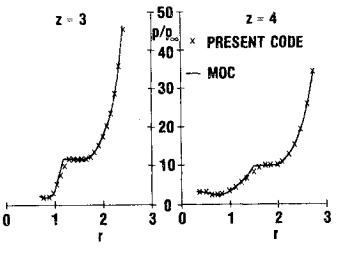

Fig. 8 Pressure profiles on expansion body; $M_\infty = 20$, $\alpha = 0$ deg.

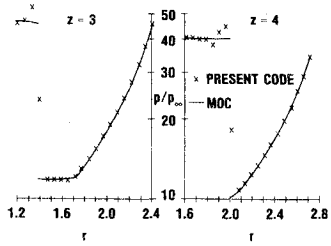

Fig. 9 Pressure profiles on compression body; $M_\infty = 20$, $\alpha = 0$ deg.

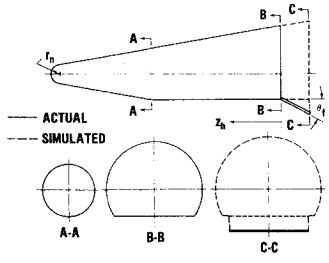

Fig. 10 Actual and simulated SCFF body (not to scale).

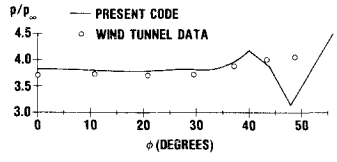

Fig. 11 Spanwise surface pressure on flat at $z_n/r_n = 1$; SCFF body, $M_\infty = 8$, $\alpha = 10$ deg.

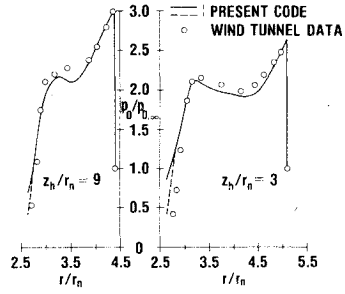

Fig. 12 Pitot pressure (p_0) profiles on flat at $\phi = 0$ deg; SCFF body, $M_\infty = 8$, $\alpha = 10$ deg.

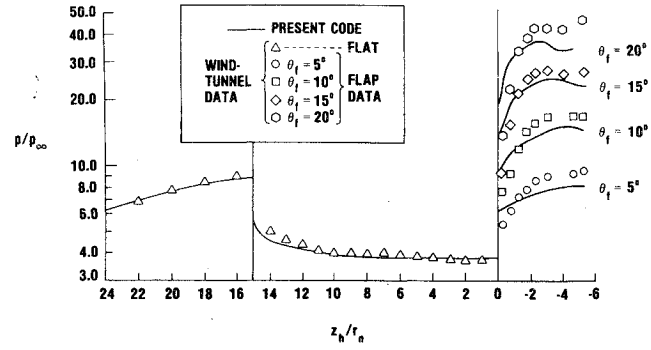

Fig. 13 Surface pressure distribution on $\phi = 0$ deg; SCFF body, $M_\infty = 8$, $\alpha = 10$ deg.

with a smooth variation to a maximum of $\Delta\phi \simeq 16$ deg at $\phi \simeq 180$ deg).

To test the validity of our basic approach for bodies with discontinuous slopes, the present method has been compared with an axisymmetric method of characteristics[19] (MOC) which has provisions for inserting expansion and fitted shock waves at body corners. Two comparisons are presented here—one for an expansion body (see Fig. 6) and one for a compression body (see Fig. 7). Figures 6 and 7 show that, in these cases, the present method correctly determines both the jumps in, and the downstream variation of, the surface pressure. In the expansion problem, the present method predicts a slightly more rapid recompression then the MOC (see Fig. 6). Also, the lower edge of the expansion fan is slightly rounded (see Fig. 8) by the present method. Figure 9 shows the numerical pressure profiles which are typical of a "captured" internal shock wave of this strength.

To illustrate the utility of the present code for a realistic three-dimensional case, a prototype lifting re-entry vehicle shape has been considered. The numerical results are compared to wind-tunnel data supplied to us by the Air Force.[20] The wind-tunnel model is shown schematically in Fig. 10. It is a sphere-cone with a flat and a flap (designated herein as SCFF). The flap consists of a finite span plate attached so that the trailing edge of the flat is the hinge line. For computational purposes this shape is simulated by extending the cone-flat and replacing the plate by a finite span wedge (Fig. 10). For the calculations, the simulated shape is expressed exactly by piecewise analytical formulas. The calculations were performed using a mesh with 15 radial points and 33 unevenly distributed meridional planes (i.e., uniform with $\Delta\phi = 4$ deg in the interval 0 deg $\leq \phi \leq 92$ deg smoothly increasing to $\Delta\phi \simeq 16$ deg at $\phi = 180$ deg). For the results presented here, the wall entropy reduction option (see Sec. IV) was used. This was necessary because the basic scheme produced subsonic axial flow on the flap surface at the larger deflection angles. Figure 11 shows the spanwise distribution of surface pressure on the flat at $z_h/r_n = 1$. At this station the edge of the flat lies between $\phi = 52$ deg and $\phi = 56$ deg. Pitot pressure profiles on the flat at $\phi = 0$ deg are shown in Fig. 12. The values computed at the wall using the entropy reduction option are higher than those obtained by using the basic wall point scheme (these latter values are indicated by the dashed lines in Fig. 12). Surface pressure distributions along the windward streamline are shown in Fig. 13. The case with the 20-deg flap deflection was terminated roughly a half-nose radius before the end of the flap due to the appearance of subsonic axial flow at the bow shock wave.

Acknowledgment

This work was jointly supported by the Naval Sea Systems Command under the Aeroballistic Re-entry Technology program and the Air Force Space and Missile Systems Organization and NSWC-IR Funds.

References

[1] Thomas, P. D., Vinokur, M., Bastianon, R., and Conti, R. J., "Numerical Solution for Three-Dimensional Inviscid Supersonic Flow," *AIAA Journal*, Vol. 10, July 1972, pp. 887-894.

[2] Morretti, G., Grossman, B., and Marconi, F., "A Complete Numerical Technique for the Calculation of Three-Dimensional Inviscid Supersonic Flows," AIAA Paper 72-192, San Diego, Calif., 1972.

[3] Moretti, G. and Pandolfi, M., "Analysis of the Inviscid Flow About a Yawed Cone, Preliminary Studies," Polytechnic Inst. of Brooklyn, Dept. of Aero. Eng. and Applied Mechanics Rept. No. 72-18, 1972.

[4] Marconi, F. and Salas, M., "Computation of Three Dimensional Flows About Aircraft Configurations," *Computers and Fluids*, Vol. 1, June 1973, pp. 185-195.

[5] Kutler, P., Reinhardt, W. A., and Warming, R. F., "Multishocked, Three-Dimensional Supersonic Flowfields with Real Gas Effects," *AIAA Journal*, Vol. 11, May 1973, pp. 657-664.

[6] Kyriss, C. L. and Harris, T. B., "A Three-Dimensional Flow Field Computer Program for Maneuvering and Ballistic Re-Entry Vehicles," *Tenth U.S. Navy Symposium on Aeroballistics*, July 1975.

[7] MacCormack, R. W., "The Effect of Viscosity in Hypervelocity Impact Cratering," AIAA Paper 69-354, Cincinnati, Ohio, 1969.

[8] MacCormack, R. W. and Warming, R. F., "Survey of Computational Methods for Three-Dimensional Supersonic Inviscid Flows with Shocks," *Advances in Numerical Fluid Dynamics*, AGARD LS-64, 1973.

[9] Abbett, M. J., "Boundary Condition Calculation Procedures for Inviscid Supersonic Flowfields," *Proceedings, AIAA Computational Fluid Dynamics Conference*, Palm Springs, Calif., 1973, pp. 153-172.

[10] Kentzer, C. P., "Discretization of Boundary Conditions on Moving Discontinuities," *Proceedings of the 2nd International Conference on Numerical Methods in Fluid Dynamics, Lecture Notes in Physics*, Vol. 8, Springer-Verlag, 1971, pp. 108-113.

[11] Solomon, J. M., Ciment, M., Ferguson, R. E., Bell, J. B., and Wardlaw, A. B., "A Program for Computing Steady Inviscid Three-Dimensional Supersonic Flow on Reentry Vehicles," Naval Surface Weapons Center/White Oak Laboratory, Silver Spring, Md., NSWC/WOL TR 77-28, Feb. 1977.

[12] Chaussee, D. S., Holtz, T., and Kutler, P., "Inviscid Supersonic/Hypersonic Body Flowfields and Aerodynamics from Shock-Capturing Technique Calculations," AIAA Paper No. 75-837, Hartford, Conn., 1975.

[13] Kutler, P., Warming, R. F., and Lomax, H., "Computation of Space Shuttle Flowfields Using Noncentered Finite-Difference Schemes," *AIAA Journal*, Vol. 11, Feb. 1973, pp. 196-204.

[14] Turkel, E., "Phase Error and Stability of Second Order Methods for Hyperbolic Problems I," *Journal of Computational Physics*, Vol. 15, June 1974, pp. 226-250.

[15] Moretti, G., "Experiments in Multi-Dimensional Floating Shock-Fitting," Polytechnic Inst. of Brooklyn Dept. of Aero. Eng. and Applied Mechanics Rept. No. 73-18, 1973.

[16] Warming, R. F. and Beam, R. M., "Upwind Second-Order Difference Schemes and Applications in Unsteady Aerodynamic Flows," *Proceedings, AIAA 2nd Computational Fluid Dynamics Conference*, Hartford, Conn., 1975, pp. 17-28.

[17] Landau, L. D. and Lifshitz, E. M., *Fluid Mechanics*, Pergamon Press (Addison-Wesley), Reading, Mass., 1959.

[18] Colasurdo, G. and Pandolfi, M., "Three Dimensional Supersonic Flow About Sliced Bodies," *Prediction of Aerodynamic Loading*, AGARD N77-19990 11-01, Feb. 1977.

[19] Inouye, M., Rakich, J. V., and Lomax, H., "A Description of Numerical Methods and Computer Programs for Two-Dimensional and Axisymmetric Supersonic Flow Over Blunt-Nosed and Flared Bodies," NASA TN-D2970, 1965.

[20] Hall, D., private communication, Air Force Space and Missile Systems Organization, Los Angeles, Calif., Feb. 1976.